https://doi.org/10.1016/j.asr.2017.03.010

Generation and Characteristics of Internal Fire Whirl in a Shaft Model with Two Corner Slits under Microgravity Conditions

Y. Huo
College of Aerospace and Civil Engineering
Harbin Engineering University
Harbin, Heilongjiang, China

W.K. Chow*
Department of Building Services Engineering
The Hong Kong Polytechnic University
Hong Kong, China

C.L. Chow
Department of Architecture and Civil Engineering
City University of Hong Kong
Hong Kong, China

*Corresponding author:
Tel: (852) 2766 5843; Fax: (852) 2765 7198
Email: beelize@polyu.edu.hk; bewkchow@polyu.edu.hk
Postal address: Department of Building Services Engineering, The Hong Kong Polytechnic University, Hunghom, Kowloon, Hong Kong.

Submitted: October 2016
Revised: March 2017

Abstract

Generation and characteristics of internal fire whirl (IFW) in a shaft model under microgravity are studied using Computational Fluid Dynamics (CFD). The shaft model has two diagonally opposite corner slits with an open roof and a 10-cm diameter heptane pool fire inside. Acceleration due to gravity is varied from normal value of g to 0.0125g. Numerical simulation indicates that even under low gravity of 0.0125g, circular air motion would still bring fuel to a high level to give a larger flame height in the shaft model, compared with that in free space under the same gravity environment, the ratio in flame height being about 1.5 except at very low gravity value. For IFW generated in the shaft model, the heat release rate, the maximum tangential velocity and the maximum axial velocity decrease slowly as gravity decreases when gravity is above 0.1g. Below 0.1g, these quantities decrease rapidly as gravity decreases. Reduction in gravity also changes the flame shape of IFW.

Keywords: shaft model, internal fire whirl, microgravity environment, simulation

1. Introduction

An internal fire whirl (IFW) can be generated [1] by a small pool fire in a shaft model with appropriate sidewall ventilation provision. Buoyancy and vorticity are the two key factors [2] in generating an IFW. For pool fire burning under normal gravity with acceleration due to gravity g, buoyancy is strong enough. With the growing interest in space exploration, fire safety in space [3] is attracting more attention. Under microgravity environment with gravity acceleration substantially less than g, the buoyancy effect on swirling flame will be significantly reduced. Vorticity due to the limitation of air motion by the shaft wall then has a stronger effect on the characteristics of an IFW. It is interesting to study the characteristics of an IFW by reducing the acceleration due to gravity from the normal value g to smaller values that would be encountered in aerospace projects.

Studies of pool fires burning under different values of gravity were reported in the literature, including numerical simulations and experimental investigation such as in fall tower with gravity down to $0.5g$ [e.g. 4-7]. However, there are very few works on study of an IFW under microgravity environment, though there might be long shaft linking chambers together in sky laboratories in space exploration projects. In this paper, characteristics of an IFW under microgravity conditions by a pool fire in a shaft model are studied using the Computational Fluid Dynamics (CFD) [8] tool Fire Dynamics Simulator (FDS).

2. Methodology

2.1 Experiment under Normal Gravity

Experiment on characteristics of an IFW in a shaft model with an open roof under normal

gravity was reported [9]. The shaft was 2 m in height and 0.32 m x 0.32 m in cross-section, with two vertical natural gaps of width 0.03 m at diagonally opposite corners (Fig. 1).

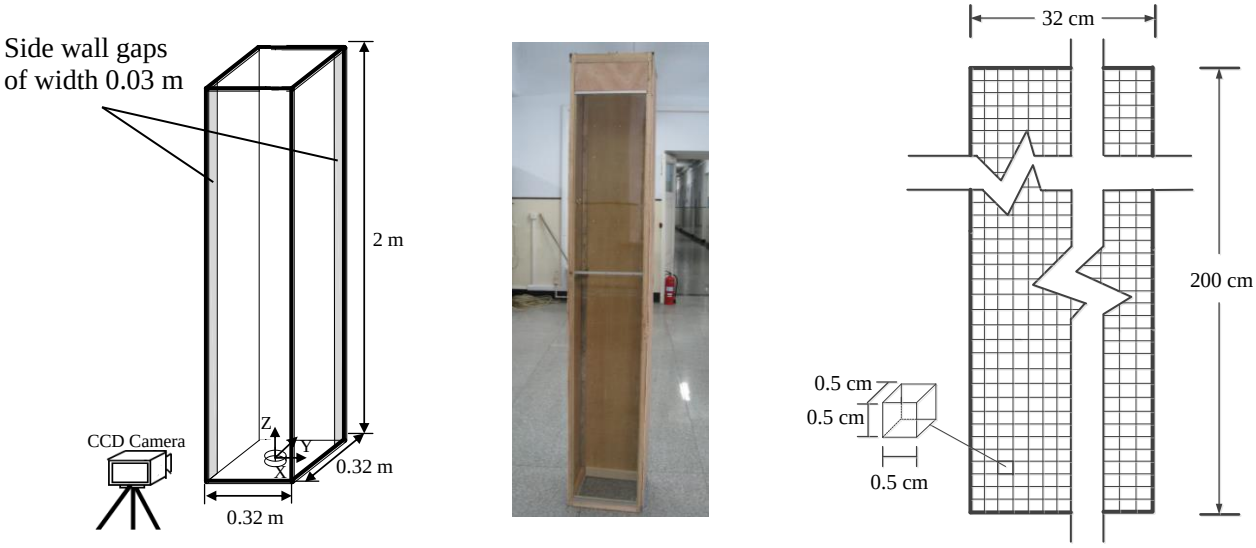

(a) Schematic (b) Photograph (c) CFD computational dimensions

Fig. 1: Experimental rig by Huo et al. (2014)

A 10-cm diameter pool fire using 25 ml 97% N-heptane was situated centrally at the bottom of the shaft, with ambient temperature lying between 21°C and 22°C. The arrangement is similar to many others' works reported in the literature [10,11]. Experimental results [9] of average air temperature as a function of height are shown in Fig. 2.

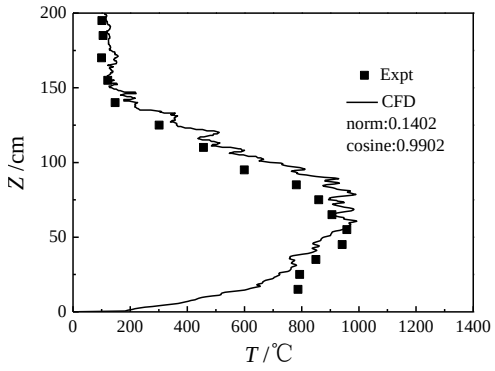

Fig. 2: Average temperature under normal gravity

The configuration above is used to study microgravity effect on the characteristics of an IFW by CFD-FDS in the present investigation.

2.2 Numerical Simulation

The CFD-based software FDS (verison 4.07) [8] is used to study IFW generated in a shaft model. Trial runs with updated versions did not give converged results and so the earlier version FDS 4.07 was taken as the simulation tool in this study. A mixture fraction combustion model with a single-step chemical reaction is assumed. Oxygen consumption method of generating 1.31×10^{3} kJkg^{-1} [12] of heat is used. Clausius-Clapeyron pressure equation [13] is used to study fuel vapor pressure above the pool surface:

$$P_{cc} = P_0 \exp\left(\frac{-M_F H_v}{\Re}\left(\frac{1}{T_{cc}} - \frac{1}{T_{boil}}\right)\right) \qquad (1)$$

In the above equation, $\Re$ is the gas constant; T_{cc} is the pool surface temperature, H_v is the heat of evaporation of N-heptane (480 kJkg^{-1}), M_F is the fuel molecular weight, T_{boil} is the boiling temperature of N-heptane (98.4℃), and P_0 is the atmospheric pressure (101.325 kPa).

The heat of combustion is modified slightly by the amount of energy released per unit mass of oxygen consumed (ΔH_{O_2} =1.31×10^{3} kJkg^{-1}) due to the presence of soot and carbon monoxide:

$$\Delta H = \frac{\nu_{O_2} M_{O_2}}{\nu_F M_F} \Delta H_{O_2} \quad (2)$$

In the above equation, ν_F and ν_{O_2} are the stoichiometric coefficients for the overall combustion process that reacts fuel with oxygen, M_{O_2} is the oxygen molecular weight. The fraction of fuel mass converted to smoke particulate is assumed to be 0.01, and the fraction of fuel mass converted into carbon monoxide can be obtained using the calculation method developed by Köylü and Faeth [14].

Physical properties of N-heptane fuel are: density = 680 kgm^{-3}, specific heat capacity = 2.2 $kJkg^{-1}K^{-1}$ [15], thermal conductivity = 0.14 $Wm^{-1}K^{-1}$, and liquid thickness = 0.02 m. The liquid fuel is taken as a thermally-thick solid. Heat lost into the liquid through conduction is calculated using the one-dimensional heat transfer equation. The fuel is assumed to burn once starting the simulation.

The Smagorinsky subgrid-scale model [16] is introduced in FDS to close the filtered equations with Smagorinsky constant *C*s of 0.2. Thermal radiation is solved using a method similar to the finite-volume method. The speed in the boundary layer and the viscous stress are calculated based on the Werne and Wengle boundary layer model [17]. Boundary conditions adopted in the shaft model for CFD numerical simulation are: wooden wall density = 545 kgm^{-3}, the specific heat capacity of wood = 1.21 $kJkg^{-1}K^{-1}$, and the thermal conductivity = 0.14 $Wm^{-1}K^{-1}$. The density, specific heat capacity and thermal conductivity of glass wall at front of the shaft are taken to be: 2700 kgm^{-3}, 0.76 $Wm^{-1}K^{-1}$ and 0.84 $kJkg^{-1}K^{-1}$, respectively. The wall is assumed to be no-slip, thermally conductive and not ignited due to low air temperature. The thickness of wooden wall and glass wall is 0.005 m,

and a one-dimensional heat conduction model is used to calculate the wall heat loss. The pressure in the extended area is set at 1 atmospheric pressure.

The computational domain of the shaft model shown in Fig. 1 has 1,638,400 cells, each of dimensions 5 mm × 5 mm × 5 mm, with sides parallel to the coordinate axes.

Gravity values from 0.0125g (0.1225 ms^{-2}) to g (9.8 ms^{-2}) are put into the air flow equations for studying buoyancy effect on IFW under microgravity environment.

The experimental and CFD-FDS numerical values of temperatures at different heights in an IFW generated under normal gravity are also shown in Fig. 2. Numerical values X_N and experimental values X_E are used in calculating the norm and the cosine as suggested in Ref. [18].

$$\text{norm} = \frac{\left\| \vec{X}_E - \vec{X}_N \right\|}{\left\| \vec{X}_E \right\|} = \frac{\sqrt{\sum_{i=1}^{n} \left(X_{Ei} - X_{Ni} \right)^2}}{\sqrt{\sum_{i=1}^{n} \left(X_{Ei} \right)^2}} \tag{3}$$

$$\text{cosine} = \frac{\left\langle \vec{X}_E, \vec{X}_N \right\rangle}{\left\| \vec{X}_E \right\| \left\| \vec{X}_N \right\|} = \frac{\sum_{i=1}^{n} X_{Ei} X_{Ni}}{\sqrt{\sum_{i=1}^{n} X_{Ei}^2 \sum_{i=1}^{n} X_{Ni}^2}} \tag{4}$$

Values of the norm and cosine on the above similarities with different grid sizes under normal gravity are shown in Table 1. The CPU times for 1 s simulation in a desktop computer with CPU of Intel (R) 2.00 GHz, RAM 64 GB are also shown in Table 1. Although the computational time is short and down to 0.42 min for grid size greater than 10 mm, the predicted results did not agree well with experiments, with norm of 0.54 and

cosine 0.90 for 20 mm grid size. For finer grids, predicted results agreed better with experiments. The computational times were much longer, up to 1342 minutes for 4 mm grid size, with norm of 0.14 and cosine of 0.99. Therefore, a suitable grid size is taken to be 5 mm × 5 mm × 5 mm in this study.

It is observed from Fig. 2 that the CFD-FDS simulation could give fairly good predictions on air temperature under normal gravity. Thus, the CFD-FDS software is employed in studying pool fires in a shaft model under microgravity environment in the present study.

Table 1 Comparison of results and consuming time for different grid sizes

Dimensions of computational cell	Total number of cells	norm	cosine	CPU time for 1 s simulation
20 mm × 20 mm × 20 mm	25,600	0.54	0.90	0.42 min
10 mm × 10 mm × 10 mm	204,800	0.32	0.99	28 min
5 mm × 5 mm × 5 mm	1,638,400	0.14	0.99	529 min
4 mm × 4 mm × 4 mm	3,200,000	0.14	0.99	1342 min

3. Results and Discussions

3.1 Buoyancy Effect on Heat Release Rate of Pool Fires

The heat release rate of liquid fuel $\dot{Q}$ was calculated by CFD-FDS using the local oxygen consumption model. Fuel vapor pressure of the fuel vapor above the surface is predicted and compared with equation (1) first. The energy consumed for evaporating liquid fuel Q_P is then adjusted based on the comparison result. The evaporation rate of the fuel is then

calculated. The mass flux of liquid fuel evaporation $\dot{m}''_{\mathrm{F}}$ can be obtained by:

$$\dot{m}''_{\mathrm{F}} = \frac{Q_P}{\Delta H_v} \quad (5)$$

The evaporated fuel mass participating in combustion is determined by the heat of vaporization, assuming that the heat release rate is directly proportional to the oxygen consumption rate, independent of the fuel involved.

Transient heat release rates of the fire in the shaft at 0.1*g*, 0.5*g* and *g* predicted by LES simulations are shown in Fig 3. Although the release rate curves have some differences at the growth stage, steady burning was observed after the ignition of the fuel for 20 s. Therefore, steady flow fields were calculated over an average of 20 s to 40 s in this paper.

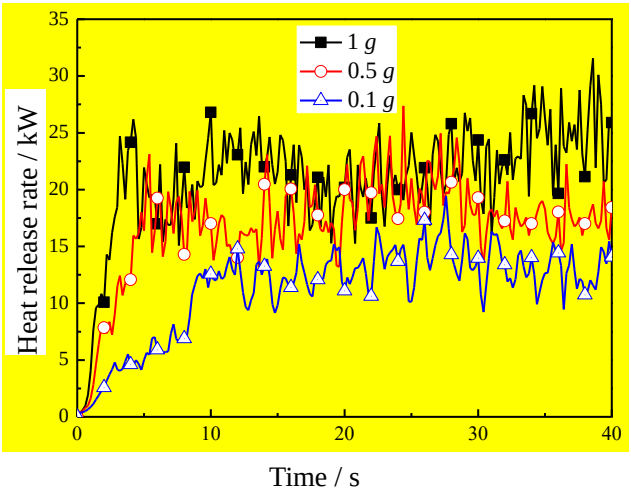

Fig. 3: Heat release rates change with time under different gravity values

Results of average heat release rates at the stable combustion phase for pool fire in free space $\dot{Q}_F$ and in the shaft model $\dot{Q}_S$ for gravity from 0.0125 *g* to 1.0 *g* are shown in Fig. 4(a). It is observed that the heat release rate in the shaft $\dot{Q}_S$ decreases as *g* decreases. Values of $\dot{Q}_S$ in the shaft model are much higher than the corresponding values for free burning $\dot{Q}_F$ at the same gravity value.

Ratio of $\dot{Q}_S / \dot{Q}_F$ at different g is shown in Fig. 4(b). It is observed that $\dot{Q}_S / \dot{Q}_F$ is about 1.5 for gravity higher than 0.4g.

The rate of change of $\dot{Q}$ with g, i.e. $\frac{d\dot{Q}}{dg}$ is shown in Fig. 4(c).

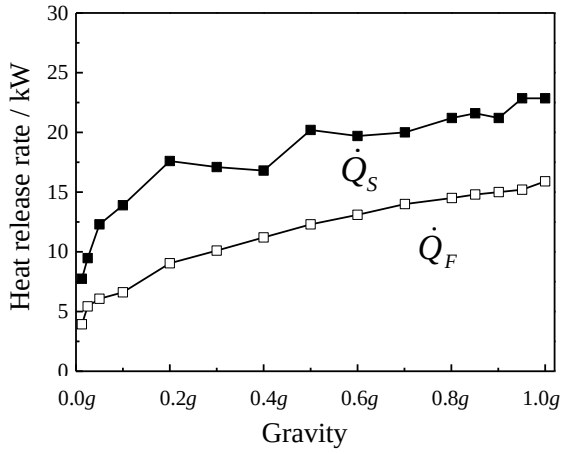

(a) Average HRR $\dot{Q}$ vs g

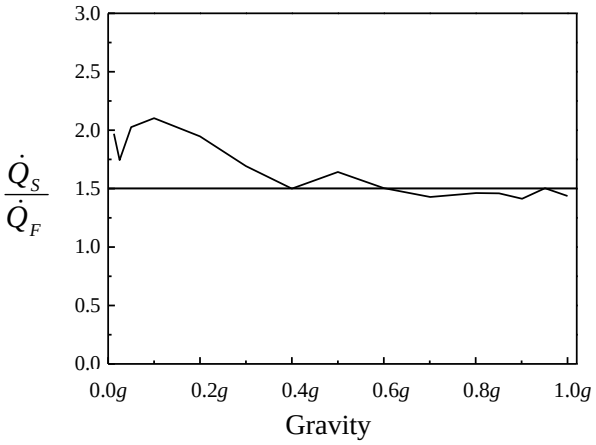

(b) Ratio R (of $\dot{Q}_S$ to $\dot{Q}_F$) vs g

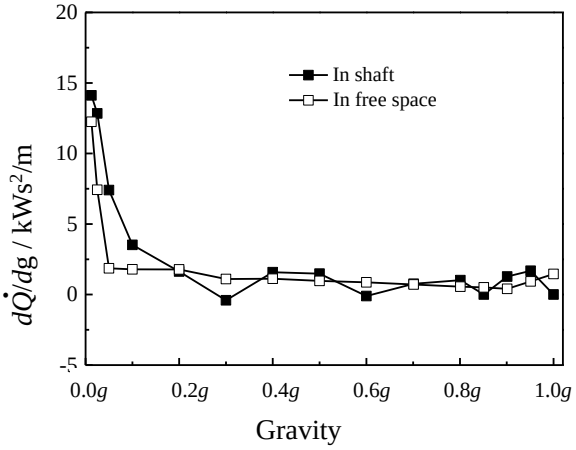

(c) Rate of change of $\dot{Q}$ with g vs g

Fig. 4: Pool fire characteristics under different gravity values

As observed from the plot of $\frac{d\dot{Q}}{dg}$ for the pool fire burning in shaft and free space in Fig.

4(c), $\frac{d\dot{Q}}{dg}$ is high, up to 12-14 kWs^2m^{-1}, at very low values of g. The values are rather constant at 2 kWs^2m^{-1} for gravity value in the range of 0.1 g to 1.0 g. This point must be watched in a pool fire burning under microgravity environment. From either Fig. 4(a) or 4(c), it can be observed that the heat release rate $\dot{Q}$ varies with gravity in two different manners. For gravity less than about 0.1 g, $\dot{Q}$ increases rapidly with g while for gravity greater than about 0.1 g, $\dot{Q}$ is roughly constant. That is to say, there are turning points in the curves in Fig. 4(a) at around 0.1 g.

3.2 Buoyancy Effect on Air Velocity

Under different microgravity environment from 0.0125g to g, the maximum upward velocity W_{max} at z = 0.5 m, 1.0 m and 1.5 m above the pool fire in the shaft is shown in Fig. 5(a). The upward velocity is reduced when g decreases due to reduction in buoyancy. The values of W_{max} are similar at lower heights of 0.5 m and 1.0 m. The value of W_{max} at height 1.5 m is significantly less than the corresponding values at lower heights, for g value greater than 0.1 g. It can be concluded that upward velocity at lower zones near to the pool fire surface is roughly constant.

The maximum tangential velocity V_{max} at z = 0.5 m, 1.0 m and 1.5 m above the pool surface is plotted as a function of g in Fig. 5(b). Again, V_{max} is reduced as g decreases. The tangential velocity of free burning flames is almost zero. The magnitude of the tangential velocity may be used to describe the rotational flow field indirectly. Similar to the variation of heat release rate, the maximum tangential velocity V_{max} decreases rapidly when g is less than 0.1 g. For V_{max} at 0.0125 g, although V_{max} drops to between 0.1 ms^{-1} and 0.2 ms^{-1} at a

height of 1.5 m, rotation is still formed in the flow field. This means internal fire whirls may be formed even under microgravity conditions.

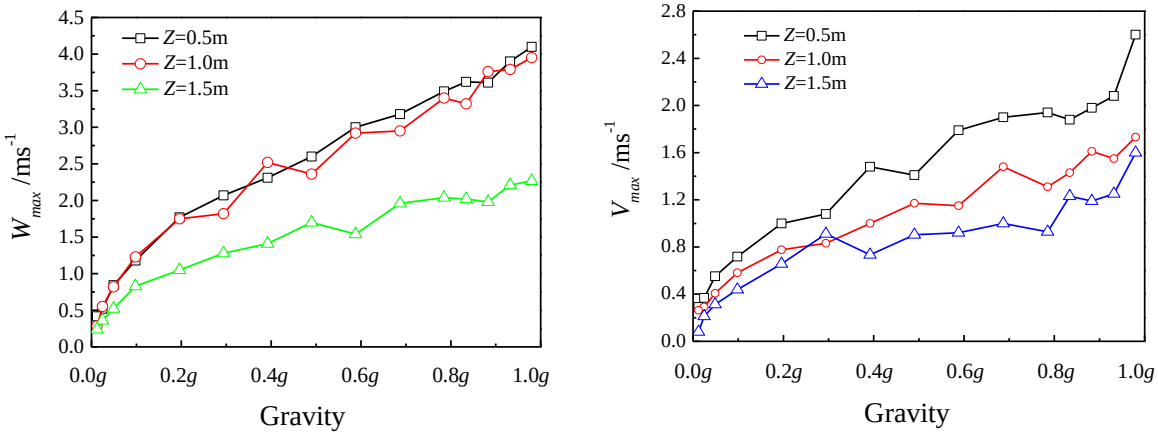

(a) Maximum upward velocity (b) Maximum tangential velocity

Fig. 5: Effect of gravity on velocity

Ratio $R_{\dot{Q}}$ of $\dot{Q}_S$ at reduced g to $\dot{Q}_S$ at normal g, for different values of g, is shown in Fig. 6. Ratio R_W of W_{max} and ratio R_{V+} and R_{V-} of V_{max} (positive and negative direction $V^{+}_{\max}$ and $V^{-}_{\min}$) at z = 0.5 m under different microgravity environment to corresponding values at normal gravity are also plotted in Fig. 6. It is seen that the general trends are similar to those for $\dot{Q}_S$, as depicted in Fig. 4(a). This suggests that there could be some correlations among $\dot{Q}_S$, W_{max} and V_{max}. IFW can be formed when the gravity is reduced to as low as 0.0125 g, even though rotation is not that vigorous in this case. V_{max} at z = 0.5 m is reduced to below 10% of V_{max} at the Earth gravity condition. The rate of change of $\dot{Q}_S$ with gravity is less than the rate of change of W_{max} and V_{max} with gravity. Each parameter decreases significantly to lower values upon reduction of gravity. Compared with the values of $\dot{Q}_S$, W_{max} and V_{max} at the Earth gravity condition, $\dot{Q}_S$ is reduced to 34% , and

W_{max} and V_{max} are reduced to 10% at 0.0125 g, respectively. $\dot{Q}_S$, W_{max} and V_{max} all decrease rapidly at gravity less than 0.1 g.

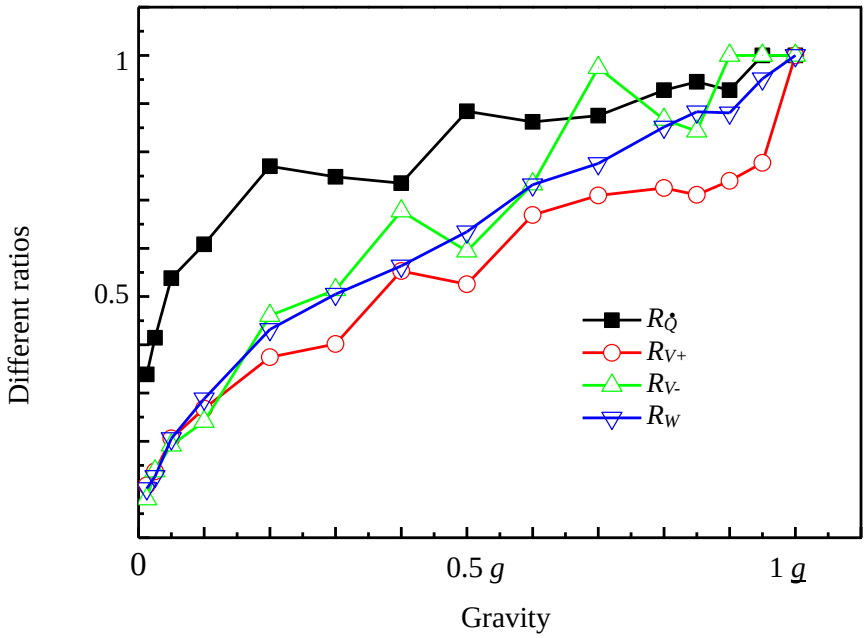

Fig. 6: Changes of ratio of heat release rate, maximum upward velocity and maximum tangential velocity with gravity (at z = 0.5 m)

Furthermore, the x coordinates of the location of the maximum tangential velocity V_{max} (represented as X) under different gravity values are shown in Fig. 7. Note that the coordinates (0,0,z) indicate the location of the central axis of the fuel pool (Fig. 1). X is in in the range 0.07-0.14 m, which is the equivalent diameter of the fuel pool. With the decrease of gravity from 1 g to 0.025 g, X only slightly increases, but then rapidly drops to a minimum at around 0.0125 g. This means that the influence of gravity only becomes evident at lower gravity values.

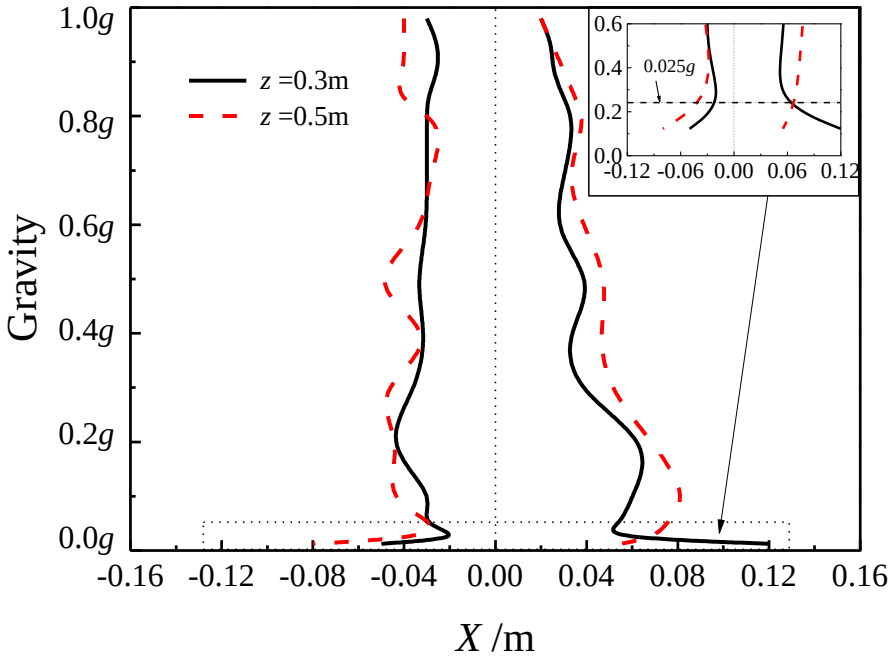

Fig. 7: Location of maximum tangential velocity

The tangential velocity V as a function of x at different z for g and 0.025 g is shown in Fig. 8. Under normal gravity g, for $z \leq 0.8$ m, the tangential velocity increases rapidly as x increases, reaches a maximum value and then decreases at about x ±0.05 m, while for z = 1.2 m, the increase is almost linear with x. On the other hand, at gravity of 0.025 g, the magnitude of tangential velocity is significantly lower compared with the corresponding values under normal gravity. Rotation is weakened, resulting in the formation of a homogenous rotating flow field.

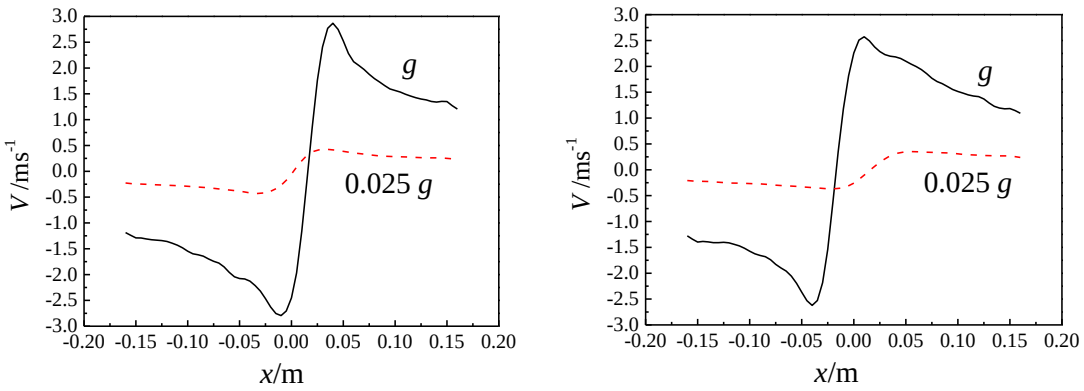

(a) z = 0.2 m (b) z = 0.4 m

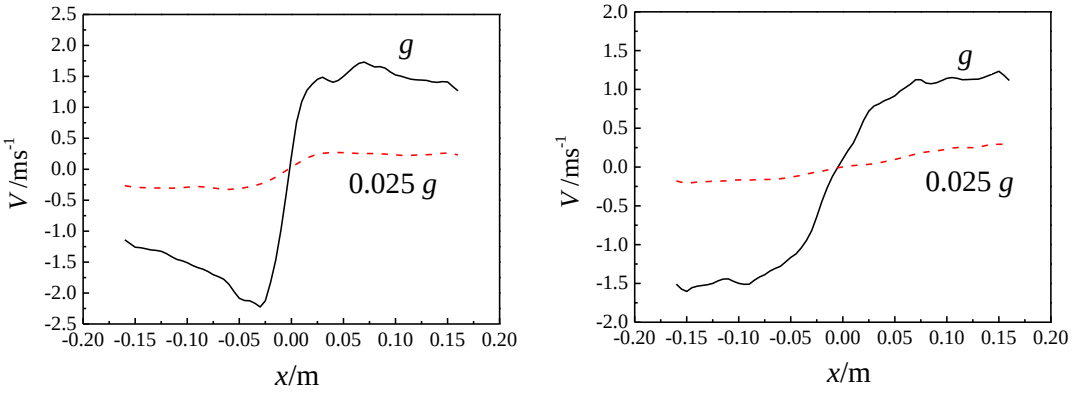

(c) z = 0.8 m (d) z = 1.2 m

Fig. 8: Tangential velocity distribution at different heights

The velocity vectors at z = 0.3 m for g, 0.5 g, 0.1 g and 0.025 g are shown in Fig. 9. It can be seen from the figure that with the decrease of gravity, rotation of the flow field became not so vigorous.

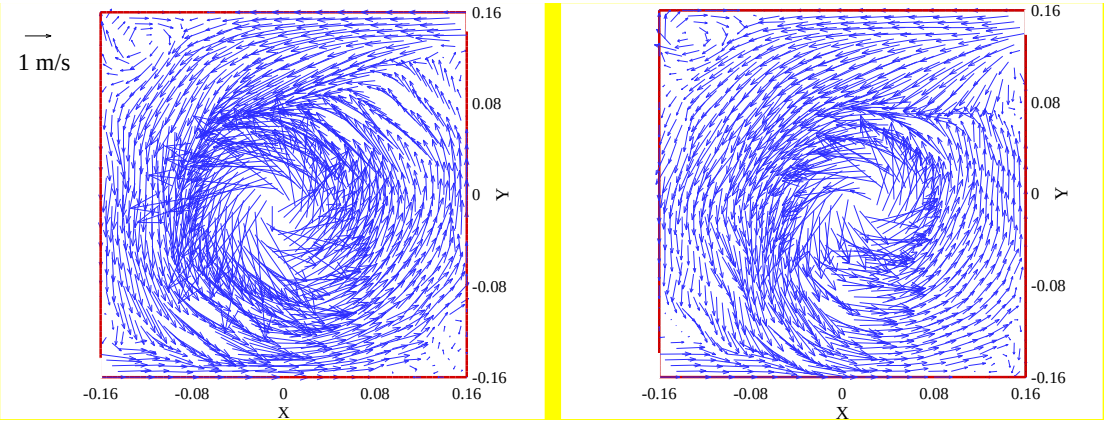

(a) At 1 g (b) At 0.5 g

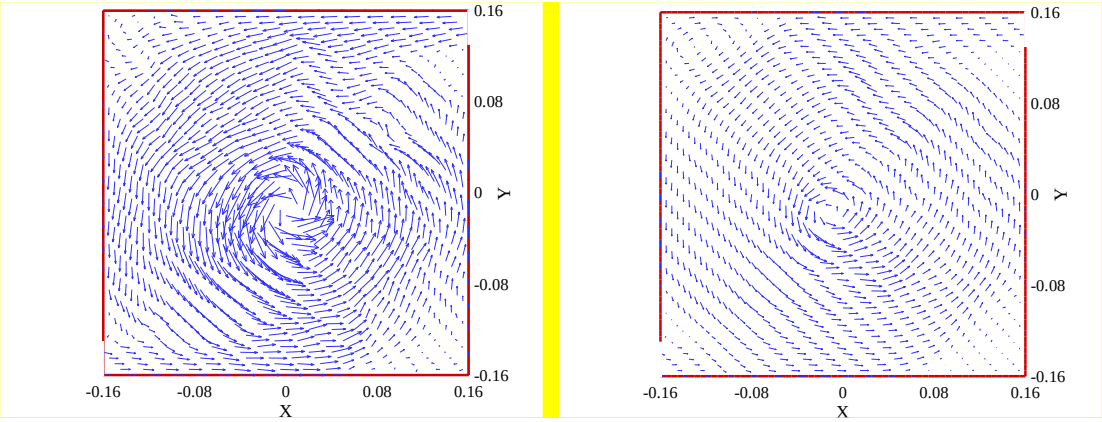

(c) At 0.1 *g* (b) At 0.025 *g*

Fig. 9: Velocity vector at *z*= 0.3 m

Variations of the ratio *V*/*W* (that is, tangential velocity/upward velocity) with *z* at *x* = 0.05 m under gravity of 0.025 *g* and *g* are shown in Fig. 10. As observed from the plots, the change of gravity does not have significant effect on *V*/*W* for the region of small *z*, indicating that both *V* and *W* change with *z* at approximately the same rate at 0.025 *g* and *g* near the flame base. However, at *z* from 0.2 m to 1.3 m, *V*/*W* is reduced at microgravity condition compared to normal gravity conditions, indicating that the fractional reduction of *V* is larger than the fractional reduction of *W* as gravity decreases.

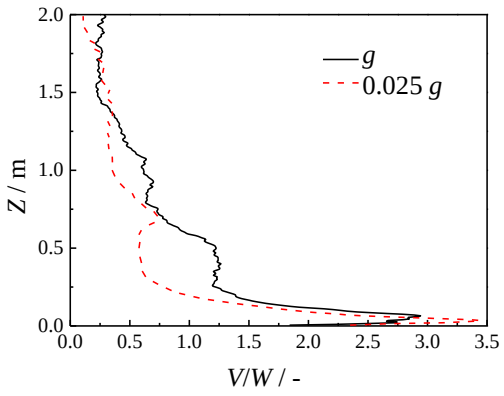

Fig. 10: *V*/*W* ratio at *x* = 0.05 m

3.3 Buoyancy Effect on Air Temperature

The maximum temperature at the central axis for the pool fire in the shaft model and in free space at different gravity values is shown in Fig. 11. It is observed that generating an IFW will give higher maximum temperatures.

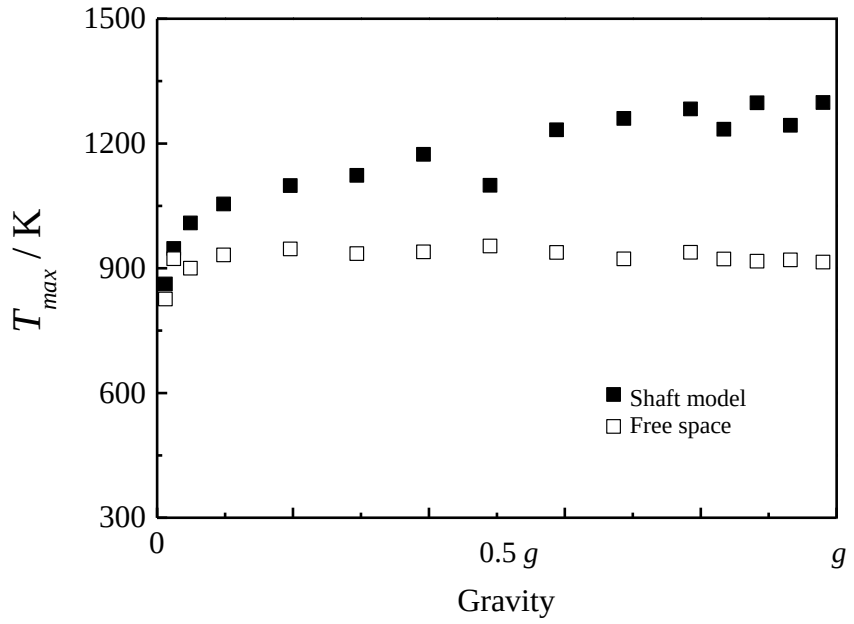

Fig. 11: Maximum temperatures on the vertical center axis under different gravity conditions

Horizontal variations of air temperature for pool fire in shaft and in free space for z = 0.3 m and 0.8 m at 0.025g, 0.1g, 0.3g, 0.5g and g are shown in Fig. 12(a) and (b). Note that the side walls of the shaft would reduce heat transfer from the domain to the outside, increasing the air temperature slightly in the shaft. As observed for from Fig. 12(a) for shaft fire, at z = 0.3 m, once the gravity decreases to 0.025g, the maximum temperature is reduced. The air temperature curve at 0.025g changes from “single peak” to “double peaks”, indicating that the high temperature zone moves away from the vertical axis of the pool fire. For the pool fire in free space, the temperature curve also exhibits “double peaks” at 0.025g. However, the maximum temperature does not decrease and the temperatures of the two

peaks are significantly higher than the temperature values at other gravity conditions. This is because in microgravity conditions, the movement patterns of the flame changes, with part of the flame reaction zone located at a different position.

At z = 0.8 m, maximum temperatures at lower gravity are lower than the maximum temperature under normal gravity as in Fig. 12 (b)(i), the maximum temperature on the central axis in free burning is significantly higher at 0.025g (Fig. 12(b)(ii)). When gravity decreases to a certain extent, part of the reacting zone moves up to give a different flame shape, thereby leading to a high temperature at higher positions. Flame shapes will be reported in greater detail in the following section.

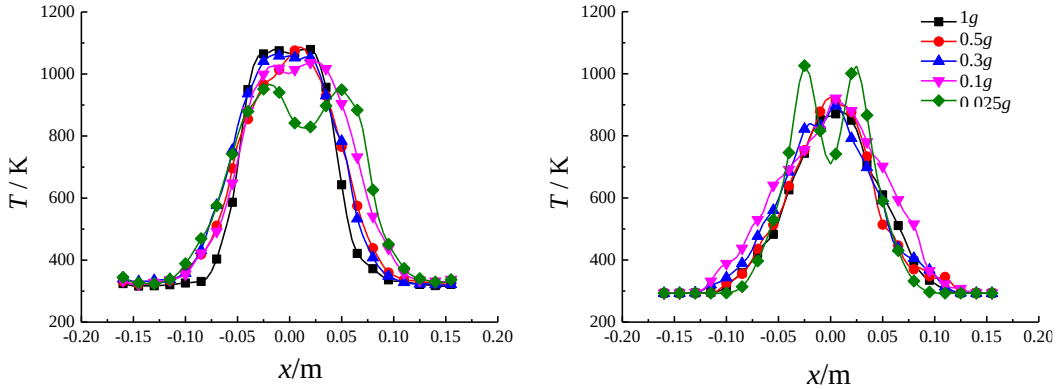

(i) In shaft model (ii) Free burning

(a) At z = 0.3 m

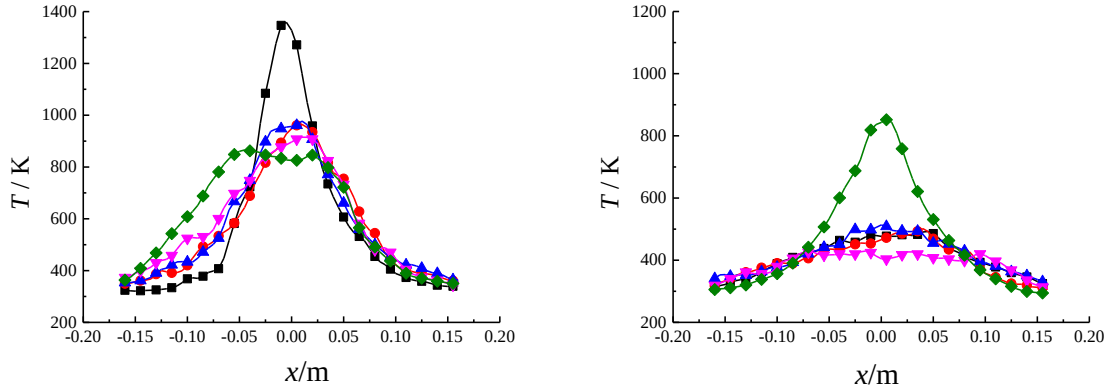

(i) In shaft model (ii) Free burning

(b) At z = 0.8 m

Fig. 12: Air temperature under different gravity

3.4 Buoyancy Effect on Flame Shape

Predicted flame shape (denoted by the estimated heat release rate per unit volume at different positions with values greater than 0 Wm^{-3}) at different gravity values are shown in Fig. 13. A schematic diagram of the predicted flame shapes is shown in Fig. 14. The flame pattern under normal gravity g was reported before [9].

When gravity is reduced, such as down to 0.025g as in Fig. 13(e), two regions are observed:

- Persistent flaming region A with strong circulation
- Intermittent flaming region B with weaker circulation

Regions A and B are redrawn schematically as shown in Fig. 14(a).

Region B is at the upper part of the flame. Rotational motion decreases with stronger diffusion and movement, leading to change in the flame shape. The upper flame moves away from the central axis to give several spiral shapes as in Fig. 14(a). The flame shape is different from an irregular spiral flame.

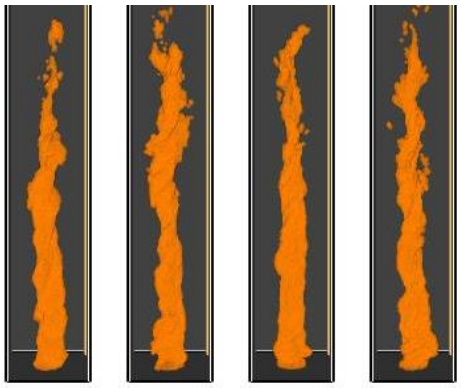

(a) In shaft at 1 *g*

(b) In shaft at 0.8 *g*

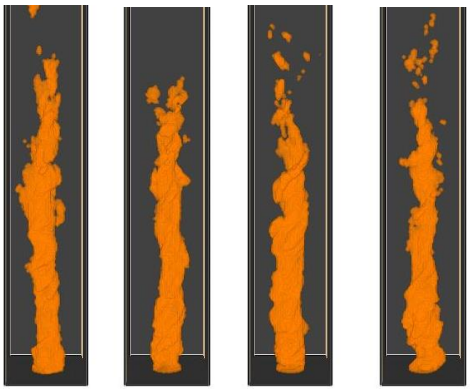

(c) In shaft at 0.5 *g*

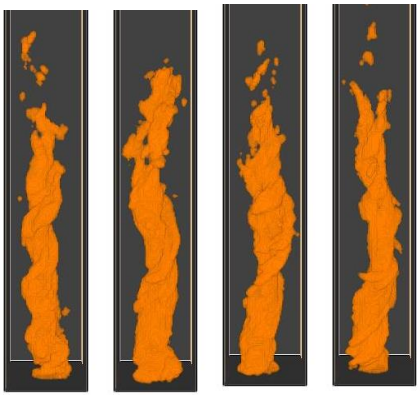

(d) In shaft at 0.2 *g*

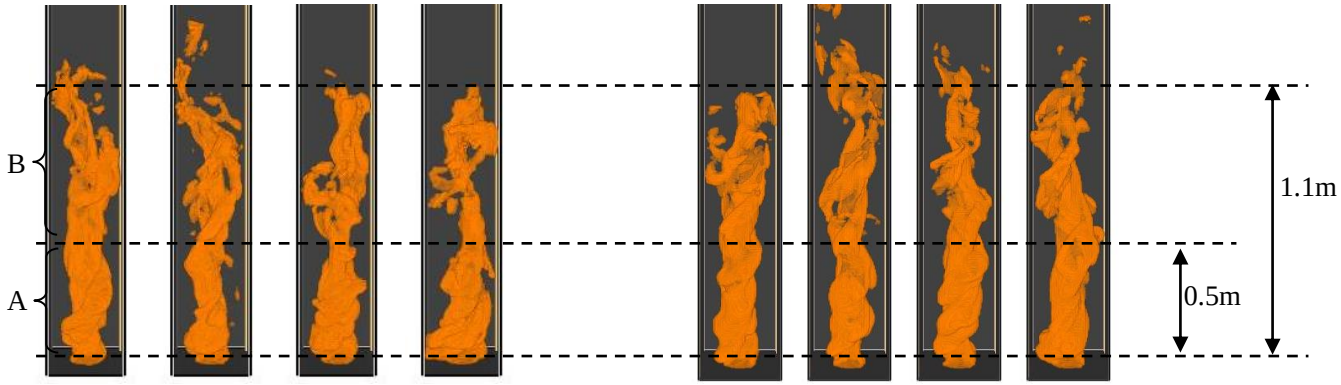

(e) In shaft at 0.025 *g*

(f) In shaft at 0.0125 *g*

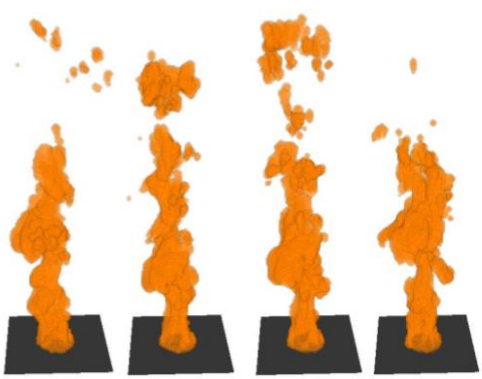

(g) Free space at *g*

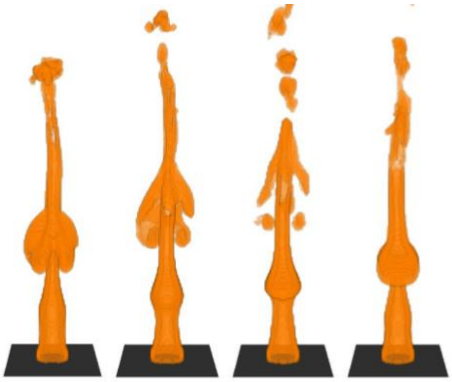

(h) Free space at 0.025 *g*

Fig. 13: Flame shapes

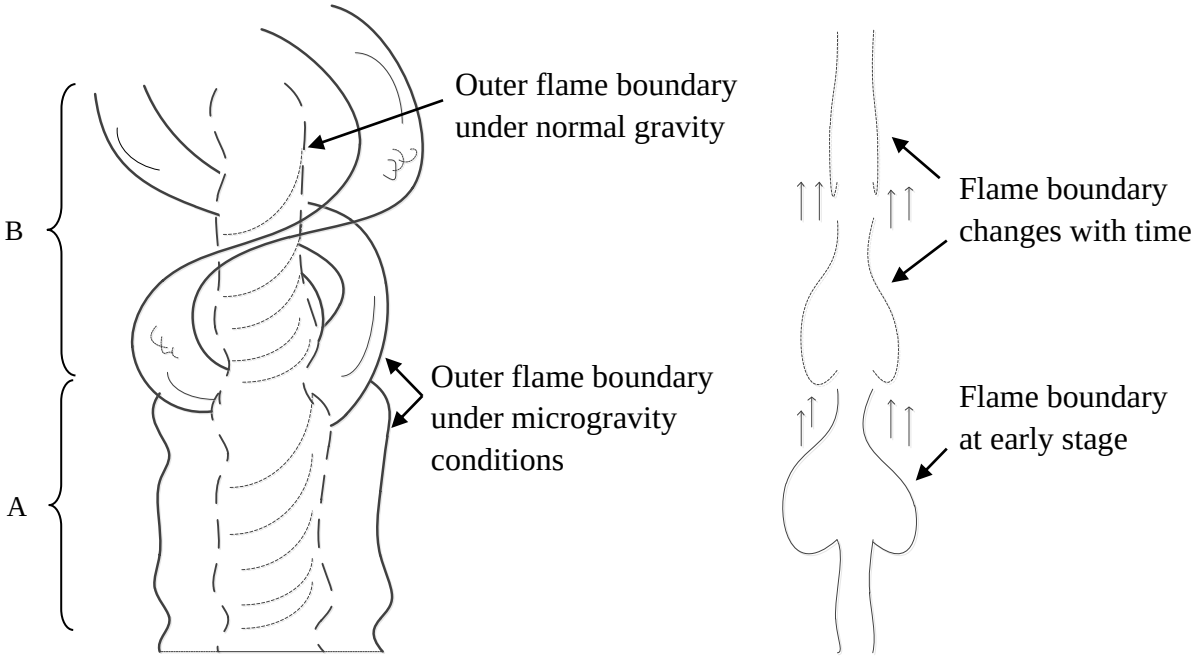

(a) In shaft (b) Free burning

Fig. 14: Flame shape in (a) shaft and (b) free space at 0.025*g*

For free burning flame, the process of flame shape change at *g* and 0.025 *g* is shown in Fig. 13(g) and Fig. 13(h). The flame movement pattern changes significantly at 0.025 *g*. A spherical flame is formed initially in the bottom region because vaporized fuel is driven by diffusion under reduction in buoyancy as shown in Fig. 14(b). With the spherical flame, before fuel exhaustion and fire extinction, the diameter of the spherical flame is diminishing. The flame gradually moves closer to the central axis. New spherical diffusion flame is generated again in the lower part and moves upwards, in a repeated manner. This explains why the temperature in the upper region is higher for pool fire burning freely under microgravity conditions.

3.5 Buoyancy Effect on Flame Height

In this paper, flame height is determined as follows: the average heat release rate per unit volume under steady burning at the central vertical axis is calculated first. The flame height is taken as the height of the position at which the average heat release rate per unit volume reduces to 0 Wm^{-3}. The flame height deduced is therefore the maximum height that the flame can move up under steady burning condition. Predicted flame heights in the shaft model H_{fi} and in free space H_{fo} at different gravity values are shown in Fig. 15. The experimental flame heights at normal gravity are also included in the figure for reference and counter-checking the reliability of the simulation. Four observations can be made from the simulation results in flame heights: (i) The flame height in the shaft obtained by simulation is roughly constant at all gravity values. (ii) The flame height in free space is also roughly constant at gravity values down to about 0.1 *g*. (iii) The flame height in the shaft is significantly higher than the flame height in free space (with a ratio of about 1.5), except at very low gravity values. (iv) There is a rapid rise in flame height in free space as gravity decreases for gravity value below 0.1 *g*. The flame height in free space approaches the flame height in shaft at very low gravity values. These observations show that gravity value does not have significant effect on flame heights in shaft, but will affect the flame height in free space at very low gravity values.

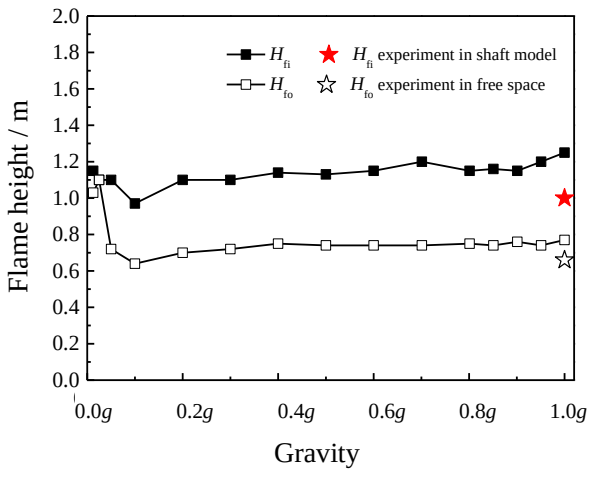

Fig. 15: Flame height in shaft and in free space

Note that for experiment with normal gravity, H_{fi} and H_{fo} are about 1 m and 0.66 m respectively, with a H_f/H_{fo} ratio of about 1.5. These values are quite close to the predicted values from CFD-FDS simulation.

4. Conclusions

Numerical simulation of internal fire whirl (IFW) in a shaft model with an open roof and two diagonally opposite corner slits is performed under different gravity values, for space fire safety investigation. The gravity values studied range from normal g to 0.0125 g. Predicted results from simulation using CFD-FDS are compared with some experimental data on liquid pool fires in the shaft model and in free space under normal gravity. The following conclusions can be drawn:

- An IFW can be generated under appropriate ventilation conditions even at low gravity value of 0.0125 g, though the circulation movement is not that vigorous.

- The flame height in the shaft is significantly higher than the flame height in free space at gravity values from 0.05 g to 1 g. The flame height in free space gradually approaches the flame height in shaft when gravity is less than 0.05 g.

- The variation of heat release rate in IFW with gravity is similar to that in free burning.

- For IFW generated in a shaft model, there exists a gravity threshold value. Above this threshold, the heat release rate, the maximum tangential velocity and the maximum axial velocity decrease slowly as gravity decreases. Below this threshold, these

quantities decrease rapidly with as gravity decreases. From the results of the present study, this gravity threshold is about 0.1 g.

- The flame shape of IFW is different from that of free burning under microgravity conditions. Spherical-shaped flame results from diffusion motion under reduction in buoyancy. When the gravity is small, the lower part of the IFW flame expands, and the compactness and continuity of flame can still be maintained. However, the upper part of the IFW forms a multi-strand intertwined and relatively dispersed irregular spiral flame.

Funding

The work described in this paper was supported by a grant from the Research Grants Council of the Hong Kong Special Administrative Region, China for the project "A study on electric and magnetic effects associated with an internal fire whirl in a vertical shaft" with account number B-Q47D and National Natural Science Foundation of China (No.51676051).

References

[1] Chow W.K., Han S.S., Experimental investigation on onsetting internal fire whirls in a vertical shaft. Journal of Fire Sciences, 2009, 27(6): 529-543.

[2] Meroney R.N., Fires in porous media: natural and urban canopies, in: Ye.A. Gayev and J.C.R. Hunt (eds.), Flow and Transport Processes with Complex Obstructions,

Springer, Chapter 8, p. 271-310 (2007).

[3] Jomaas G., Torero J.L., Eigenbrod C., et al. Fire safety in space — beyond flammability testing of small samples. Acta Astronautica, 2015, 109: 208-216.

[4] Most J., Mandin P., Chen J. et al. Influence of gravity and pressure on pool fire-type diffusion flames. Twenty-Sixth Symposium (International) on Combustion/The Combustion Institute, 1996, pp. 1311-1317.

[5] Yao W., Lu S.X., Wang J., Numerical prediction of effects of gravity on the centerline temperature and velocity of axisymmetric fire plumes, Journal of Fire Sciences, 2007, 25(5):403-423.

[6] Yoshihara N., Ito A., Torikai H., Flame characteristics of small-scale pool fires under low gravity environments, Proceedings of the Combustion Institute, 2013, 34(2): 2599-2606.

[7] Abe H., Ito A., Torikai H., Effect of gravity on puffing phenomenon of liquid pool fires, Proceedings of the Combustion Institute, 2015, 35(3): 2581-2587.

[8] McGrattan K., Fire Dynamics Simulator (Version 4) Technical Reference Guide, National Institute of Standards and Technology Special Publication 1018, March 2006.

[9] Huo Y., Zou G.W., Li S.S., Gao Y., Characteristics of fire whirls induced by liquid fuel in a vertical shaft, Journal of Harbin Institute of Technology, 2014, 46(1): 77-82. (In Chinese)

[10] Chuah K.H., Kuwana K., Saito K., Williams F.A., Inclined fire whirls, Proceedings of the Combustion Institute, 2011, 33: 2417-2424.

[11] Saito K., Cremers C.J., Fire-whirl enhanced combustion, Proceedings of the Joint ASME/JSME Fluids Engineering Conference, ASME FED, 1995, Vol. 220.

[12] Huggett C., Estimation of rate of heat release by means of oxygen consumption measurements, Fire and Materials, 1980, 4(2): 61-65.

[13] Prasad K., Li C., Kailasanath K., Ndubizu C., Ananth R., Tatem P.A. Numerical modelling of methanol liquid pool fires. Combustion Theory and Modelling, 1999, 3(4): 743-768.

[14] Ü. Ö. Köylü and G. M. Faeth. Carbon Monoxide and Soot Emissions from Liquid-Fueled Buoyant Turbulent Diffusion Flames. Combustion and Flame, 1991, 87(1): 61–76.

[15] Zábranský M., Růžička V., Heat capacity of liquid n-heptane converted to the international temperature scale of 1990, Journal of Physical and Chemical Reference Data, 1994, 23(1):55-61.

[16] Smagorinsky J., General circulation experiments with the primitive equations: part I, The basic experiment, Monthly Weather Review, 1963, 91(3): 99-164.

[17] Werner H., Wengle H., Large-eddy simulation of turbulent flow over and around a cube in a plate channel, In 8th Symposium on Turbulent Shear Flows, Munich, Germany, 1993: 155-168.

[18] Peacock R.D., Reneke P.A., Davis W.D., Jones W.W., Quantifying fire model evaluation using functional analysis, Fire Safety Journal, 1999, 33: 167-184.